2

Physics-Based Control Methods

T. A. Sands
Columbia University,
USA

1. Introduction

Spacecraft control suffers from inter-axis coupling regardless of control methodology due to the physics that dominate their motion. Feedback control is used to robustly reject disturbances, but is complicated by this coupling. Other sources of disturbances include zero-virtual references associated with cascaded control loop topology, back-emf associate with inner loop electronics, poorly modeled or un-modeled dynamics, and external disturbances (e.g. magnetic, aerodynamic, etc.). As pointing requirements have become more stringent to accomplish missions in space, decoupling dynamic disturbance torques is an attractive solution provided by the physics-based control design methodology. Promising approaches include elimination of virtual-zero references, manipulated input decoupling, which can be augmented with disturbance input decoupling supported by sensor replacement. This chapter introduces these methods of physics-based control. Physics based control is a method that seeks to significantly incorporate the dominant physics of the problem to be controlled into the control design. Some components of the methods include elimination of zero-virtual reference, observers for sensor replacements, manipulated input decoupling, and disturbance-input estimation and decoupling. In addition, it will be shown that cross-axis coupling inherent in the governing dynamics can be eliminated by decoupling a normal part of the physics-based control. Physics-based controls methods produce a idealized feedforward control based on the system dynamics that is easily augmented with adaptive techniques to both improve performance and assist on-orbit system identification.

2. Physics-based controls

2.1 Zero-virtual references

Zero-virtual references are implicit with cascaded control loops. When inner loops reference signals are not designed otherwise, the cascaded topology results in zero-references, where the inner loop states are naturally zero-seeking. It is generally understood that if any control system demands a positive or negative rate, the inner position loop (seeking zero) would essentially be fighting the rate loop, since a positive or negative rate command with quiescent initial conditions dictates non-zero position command. Elimination of the zero-virtual reference may be accomplished by using analytic expressions for both position and rate eliminating the nested, cascaded topology. Using analytic expressions for both position and rate commands implies the utilization of commands that both correspond to achieving

the same desired end state, essentially eliminating the conflict between the position and rate commands inherit in the cascaded topology.

2.2 Manipulated Input Decoupling (MID)

Manipulated input is the actual variable that can be modified by a control design. Very often in academic settings control u is the goal of a design, but in reality a voltage command is sent to a control actuator, and this voltage command should be referred to as the true manipulated input. The importance of this distinction lies in the fact that electronics may not properly replicated the desired control u, unless the control designer has accounted for internal disturbance factors like the resistive effects of back-emf (inherit in any electronic device where current is generated and modified in the presence of a magnetic field). The manipulated input signal should be designed to decouple these effects.

2.3 Sensor replacement

Due to simplicity of the approach, observer-based augmentation of motion control systems is becoming a ubiquitous method to increase system performance [4], [8], [11], [12]. The use of observers also permits (in some cases) elimination of hardware associated with sensors, or alternatively may be used as a redundant method to obtain state feedback. Velocity sensors may be eliminated using speed observers based on position measurement without. Estimation methods such as Gopinath-styled observers and Luenberger-styled Observers are robust to parameter variation and sensor noise. Both position and velocity estimates may be used for state feedback eliminating the effects of sensor noise on the state feedback controller. Luenberger-styled and Gopinath-styled observer topologies will be compared. Luenberger-styled observers (henceforth simply referred to as Luenberger observers) are a simple method to estimate velocity given position measurements that will prove superior to Gopinath-styled observers (which remain a viable candidate for sensor replacement). Additionally, the Luenberger observer may be used to provide estimates of external system disturbances, since the observer mimics the order of the actual systems dynamic equations of motion. When used the Luenberger disturbance observer bestows robustness to system parameter variations.

Often used terminology from current literature [11], [12] is maintained in here where the modification of the signal chosen as the disturbance estimate establishes a "modified" Luenberger observer. The modified Luenberger observer as referred in the cited literature is clearly superior (with respect to disturbance estimation) to the nominal Luenberger observer, so it is assumed to be the baseline Luenberger observer for disturbance estimation. Recent efforts [12], [14] seeking to improve estimation performance augments the architecture with a second, identical Luenberger observer. The two observers are tuned to estimate velocity and external disturbances respectively. The approach improves estimation accuracy and system performance, but still suffers from estimation lag, motivating these more recent improved methods eliminating estimation lag. Methods to improve estimation performance will be presented. Together with estimation improvement, motion control will be enhanced with disturbance input decoupling (which also aids estimation performance).

2.4 Disturbance Input Decoupling (DID)

Augmentation of speed observers with a command feedforward path permits near-zero lag estimation, even in a single-observer topology. Elimination of estimation lag improves

estimation accuracy which subsequently improves the performance of the motion controller. Augmentation of the motion controller with disturbance input decoupling extends the bandwidth of nearly-zero lag estimation considerably again even in a single-observer topology. The estimates from the observer are frequently used for state feedback eliminating the requirements for both velocity sensors and position measurement smoothing. Adding command feedforward to the observer establishes nearly-zero lag estimation with good accuracy. Furthermore, augmenting the motion controller with disturbance input decoupling improves motion control.

2.5 Idealized feedforward control based on predominant physics

Decoupling the cross-motion motivates an idealized feedforward control. Section 7 of this chapter will introduce a feedforward control for accomplishing commanded trajectories that is designed using the predominant physics and decouples the particular solution to the differential equation of motion that results from the commanded trajectory.

2.5.1 Cross-axis motion decoupling

Newton's Law is commonly known: the sum of forces acting on a body is proportional to its resultant acceleration, and the constant of proportionality is the body's mass. This applies to all three axes of motion for 3-dimensional space, so the law can also be stated as "the summed force vector [3x1] acting on a body is proportional to its resultant acceleration vector [3x1], and the constant of proportionality is the body's mass matrix [3x3]". One crucial point is that this basic law of physics applies only in an inertial frame that is not in motion itself. A similar law may be stated for rotational motion just as we have stated Newton's Law for translational motion. The rotational motion law is often referred to as Newton-Euler, and it may be paraphrased as: "the summed torque vector [3x1] acting on a body is proportional to its resultant angular acceleration vector [3x1], and the constant of proportionality is the body's mass inertia matrix [3x3]." Newton-Euler also only applies in a non-moving, inertial frame. The equations needed to express the spacecraft's rotational motion are valid relative to the inertial frame and may be expressed in inertia. The motion measurement relative to the inertial frame is taken from onboard sensors expressed in a body fixed frame. The resulting cross product that accounts for relative motion of the body frame contains the key cross coupled terms often casually referred to as "roll-yaw coupling" for example in the case of a spacecraft whose inertia matrix produced relatively pronounced coupling between the roll and yaw axes. Decoupling the cross-product nonlinearities eliminates undesired motion.

2.6 Reference trajectory

A reference trajectory is introduced in section 9.2 to improve performance still further. The main motivation is that a controller should recognize that the plant is not (cannot) instantaneously achieve the commanded trajectory. Time is required for motion to occur, so when it is desired to maneuver more rapidly, a reference trajectory may be used.

2.7 Adaptive control and system identification

Taken together, an idealized feedforward control (designed using the dynamics of the system) together with a classical feedback controller and a reference trajectory lead to the

ability to introduce adaptive control schemes that can learn a spacecraft's new physical parameters and adjust the control signal to accommodate things like fuel sloshing and spacecraft damage.

3. Equations of motion

Newton's Law is commonly known: the sum of forces acting on a body is proportional to its resultant acceleration, and the constant of proportionality is the body's mass. This applies to all three axes of motion for 3-dimensional space, so the law can also be stated as "the summed force vector [3x1] acting on a body is proportional to its resultant acceleration vector [3x1], and the constant of proportionality is the body's mass matrix [3x3]". One crucial point is that this basic law of physics applies only in an inertial frame that is not in motion itself. A similar law may be stated for rotational motion just as we have stated Newton's Law for translational motion.

The rotational motion law is often referred to as Newton-Euler, and it may be paraphrased as: "the summed *torque* vector [3x1] acting on a body is proportional to its resultant *angular* acceleration vector [3x1], and the constant of proportionality is the body's mass *inertia* matrix [3x3]." Newton-Euler also only applies in a non-moving, inertial frame. The equations needed to express the spacecraft's rotational motion are valid *relative to* the inertial frame (indicated by subscript "B/i" often assumed) and may be *expressed* in inertia. The motion measurement *relative to* the inertial frame is taken from onboard sensors *expressed in* a body fixed frame

$$\dot{\vec{H}} = \left\{\frac{d\vec{H}}{dt}\right\}_i = \left\{\frac{d\vec{H}}{dt}\right\}_B + \{\vec{\omega}\}^{B/i} \times \{\vec{H}\}_B \text{where } \{\vec{H}\}_B = [\mathbf{J}] \cdot \{\vec{\omega}\}^{B/i} \quad (1)$$

$$\sum\{\vec{T}\}_{B/i} \rightarrow \{\boldsymbol{\tau}\}_B = \{\dot{\mathbf{H}}\} = [\mathbf{J}]\{\dot{\boldsymbol{\omega}}\} + \{\boldsymbol{\omega}\} \times [\mathbf{J}]\{\boldsymbol{\omega}\} \quad (2)$$

Note the cross product that accounts for relative motion of the body frame contains the key cross coupled terms often casually referred to as "roll-yaw coupling" for example in the case of a spacecraft whose inertia matrix produced relatively pronounced coupling between the roll and yaw axes. Decoupling the cross-product nonlinearities eliminates undesired motion and makes the equation more similar to the basic Newton's Law in an inertial reference frame. Decoupling the cross-product may be done in feedforward or feedback fashion, but should account for both the homogenous solution to the governing differential equation (response to initial conditions) and also the particular solution (response to the command input). Well-behaved, decoupled dynamics would behave with simple double-integrator dynamics, so the mathematical expressions of force dynamics and torque dynamics would look similar.

4. Virtual-zero references and mid

Spacecraft torque-actuators contain electronic that often contain other force or torque motors. Control moment gyroscopes for example are said to exhibit "torque magnification" since a small amount of torque applied to the gimbal motor produces a resultant large spacecraft torque. Motors associated with electronics are cascaded inner-loops, and they are

often paid less attention in the control design [9], [11]. Such cascaded inner loops often reduce the overall system bandwidth due to zero-virtual references. Lacking designed references, the cascaded inner loops seek zero. Design engineers should consider eliminating zero-virtual reference and decoupling the cascaded electronics to increase overall system performance. Consider four voice-coil force actuators (as an example), and pay particular attention to the fact that force output is coupled due to back-emf and armature resistance which physically desire to seek a virtual-zero reference. In accordance with the definition of MID in section 2.4, the goal is to design the voltage signal that accounts for the predominant physics (both electrical and physical motion). The manipulated input is a voltage signal (e.g E*(s)), not control signal u.

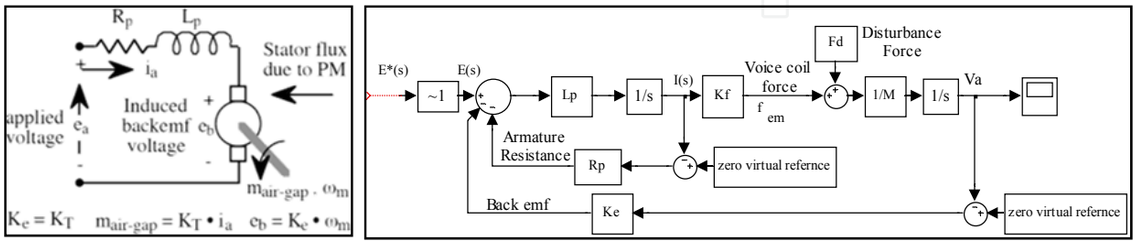

Fig. 1. LEFT: DC servo drive (cascaded current loop). RIGHT: Voice coil actuator. Note the presence of cross coupled armature resistance and back-emf.

An initial goal is to regulate i(t) to regulate f_{em}, (since i(t) and f_{em} are identical variables for this class of machines) to get well-behaved dynamics for the motion states. Since velocity-dependent back-emf complicates the electrical dynamics (it is cross-coupled state feedback), feedback decoupling was implemented. Especially since K_e and K_f are often quite high, back-emf can be quite a factor if not dealt with. Note that positive feedback for $\hat{R}_e$ approximately nulls K_e. Next, the effects of voice-coil resistance R_p were decoupled with feedback decoupling (i.e. decouple the effects of the armature resistance). Neither of these activities (decoupling back-emf and armature resistance) improves dynamics stiffness rather they yield well behaved force modulators. As a matter of fact, decoupling back-emf results in system inertia being the only remaining system disturbance rejection property.

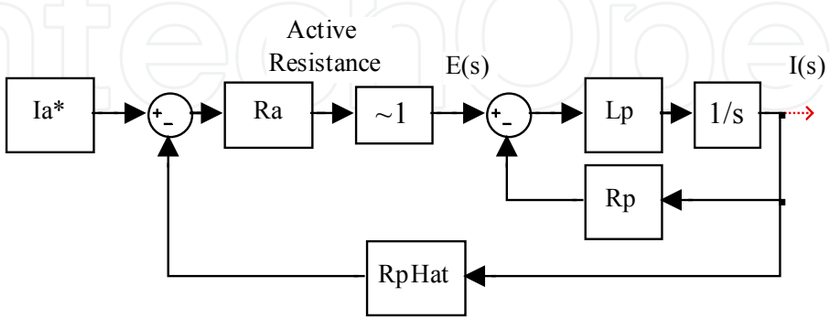

$$\frac{I(s)}{I^*(s)} = \frac{R_a}{L_p s + R_a + R_p} \rightarrow \left.\frac{R_a}{L_p s + R_a}\right|_{\hat{R}_p \rightarrow R_p} \tag{3}$$

Fig. 2. Decoupling armature resistance.

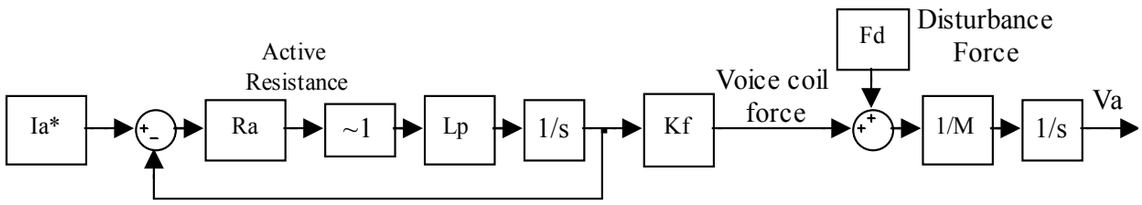

Fig. 3. Well-behaved voice coil actuator.

Figure 4 is a simplified block diagram that displays the back-emf and armature resistance decoupling (driven to near-zero). Mason's rule analysis (similar to the one done for decoupling armature resistance in Figure 2) demonstrates that decoupling yields unity gain current regulators.

Notice this remains *strictly* true as the armature resistance estimation is accurate. In reality, it is okay if it is not *strictly* true. The goal is to reduce the effects of armature resistance to allow the active resistance to dominate yielding well-behaved current regulators (i.e. within the regulators bandwidth, the behavior is nearly exactly as desired). Since these are the cascaded low energy states that feed the high energy motion states, the active resistance was tuned to a high bandwidth, 100 Hz (resulting value of R_a=4).

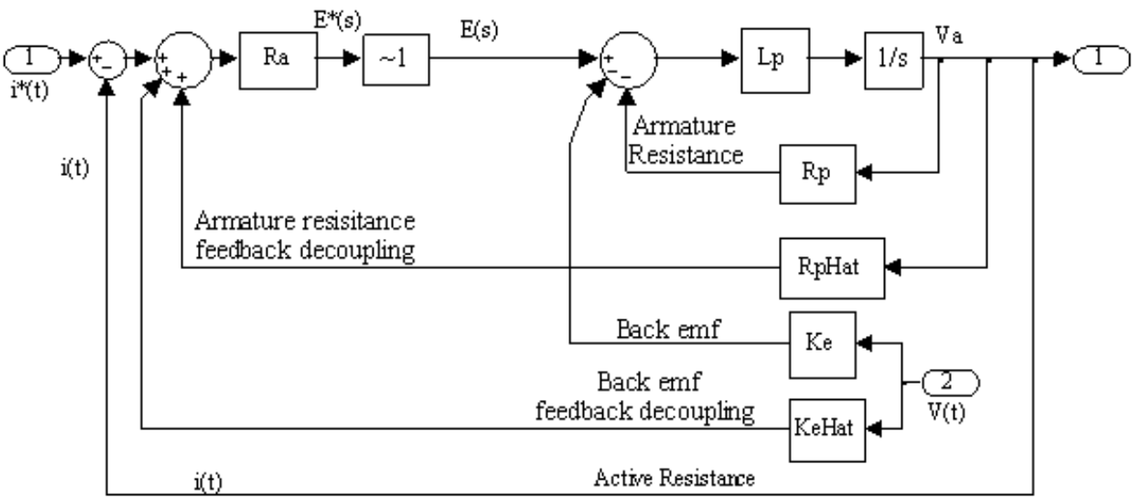

Fig. 4. Decoupling of armature resistance and back-emf.

Placing the force actuators into the equations of motion yields the following block diagram. After decoupling back-emf and armature resistance, the simplified block diagram reveals the now-dominant active resistance that may be tuned for system performance. The equivalent full-form displayed in block diagram form below.

Neglecting armature resistance and back-emf decoupling, the resultant dynamic stiffness is:

$$\frac{F_d(s)}{V(s)} = \frac{M_v L_p s^4}{(b_a s^2)+K_{rsas}+K_{risa}(L_p s-R_p)(K_f)+K_e L_p s^4} \tag{4}$$

The effects of decoupling may be observed on dynamic stiffness by setting an terms to zero to expose the individual effects of each loop on disturbance rejection.

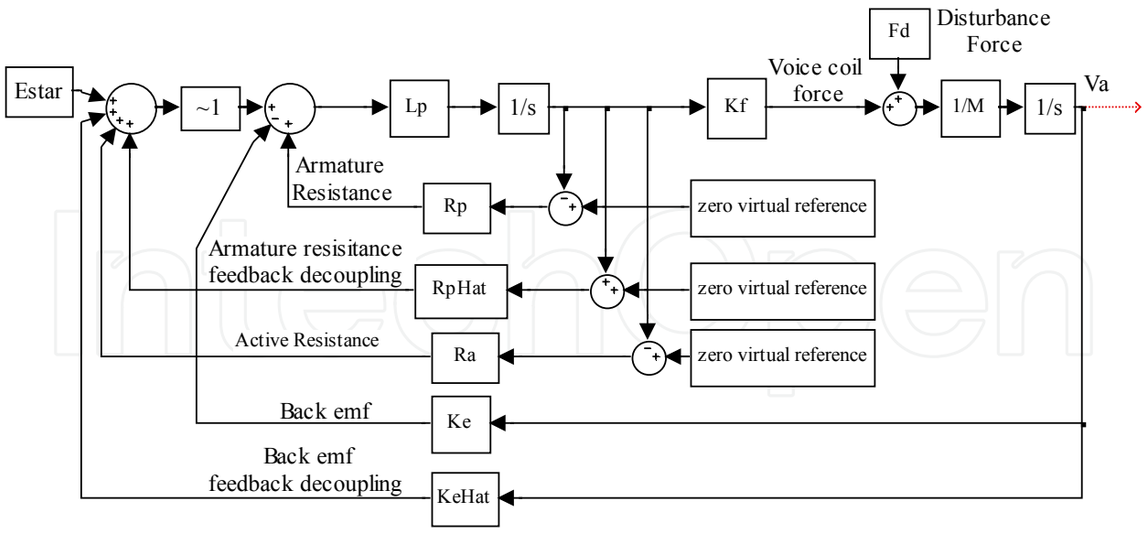

Fig. 5. Voice-coil state block diagram with virtual-zero reference.

5. Sensor replacement: Observers

This section of the paper evaluates the effect of observer types on two, observer-based, incremental motion format, state feedback motion controllers with a cascaded current loop applied to the dc servo drive in Fig. 1 with state feedback decoupling, but not disturbance input decoupling (to be performed in a later section of the paper). Luenberger and Gopinath observer topologies (Figure 6) will be compared [12], [14] (as taught in ME746 at the University of Wisconsin at Madison). Luenberger-styled observers (henceforth simply referred to as Luenberger observers) are a simple method to estimate velocity given position measurements. Additionally, the Luenberger observer may be used to provide estimates of external system disturbances, since the observer mimics order of actual systems dynamic equations of motion. When used the Luenberger disturbance observer bestows robustness to system parameter variations.

$J_p = 0.015 \times 10^{-3}$ kg m^2	polar moment of inertia
$K_T = 0.14$ Nm/Amp	torque constant
$K_e = 0.14$ volts/rad/sec	back emf constant
$R_p = 2.6$ ohms	armature resistance
$L_p = 4.3$ millihenries	armature inductance
e_s = applied terminal voltage in volts	
i_a = armature current in amperes	
m_{ag} = electromagnetic air-gap torque (moment) = $K_T\, i_a$	
e_b = induced (back emf) voltage = $K_e\, \omega_m$ in volts	
ω_m = load angular velocity in rad per sec	
θ_m = load angular position in rad	

Table 1. Parameter Values and Variable Definitions.

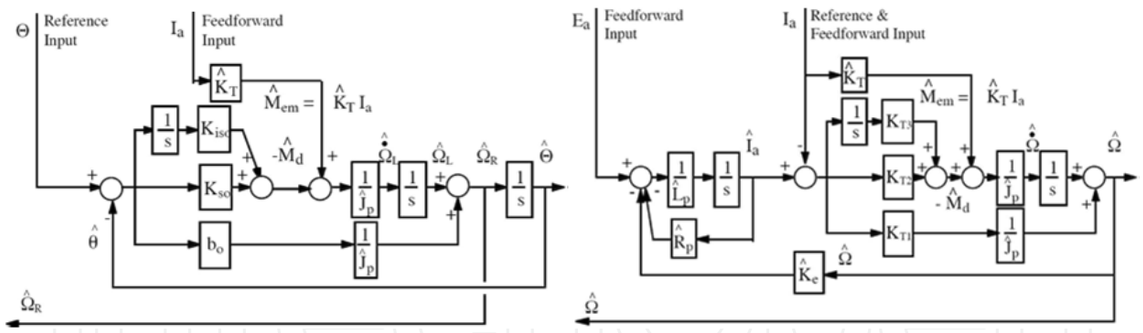

Fig. 6. LEFT: Luenberger-Styled Observer. RIGHT: Gopinath-Styled Velocity Observer.

5.1 Observer gain tuning

For desired observer eigenvalues λ_1=12.5, λ_2=50, λ_3=200, desired motion controller gains (tuned for disturbance rejection) λ_{c1}=6, λ_{c2}=25, λ_{c3}=100, and current regulator gain λ_i=800, the general form of the characteristic equation may be equated to the specific observer forms, controller form and current regulator form revealing gains. Tuning was directed in the problem statement to be identical to permit apples-to-apples comparison of effects on estimation accuracy.

5.2 Luenberger tuning (actual current)

This method uses the actual current from the actuator circuit (rather than modeled or predicted current) to provide the feedforward element of the observer. This position would normally include the actual current or control, u in typical observer designs (recalling that observer design is a *dual* process of controller design). Utilizing the reference input and actual circuit moment, you can produce an estimate of remaining disturbance (normally fed back to feedback controllers to handle).

$$\text{C.E.} = (s+\lambda_1)(s+\lambda_2)(s+\lambda_3) = \hat{J}_p s^3 + b_o s^2 s + K_{so} s + K_{iso} \tag{5}$$

$$b_o = \hat{J}_p(\lambda_1 + \lambda_2 + \lambda_3) \tag{6}$$

$$K_{so} = \hat{J}_p([\lambda_1(\lambda_2 + \lambda_3) + \lambda_2 \lambda_3] \quad K_{iso} = \hat{J}_p(\lambda_1 \lambda_2 \lambda_3) \tag{7}$$

5.3 Gopinath tuning

$$\frac{\hat{\omega}(s)}{\omega(s)} = \frac{(K_{T1}s^2 + K_{T2}s + K_{T3})\left(\frac{J_p s^2(L_p - \hat{L}_p) + J_p(R_p - \hat{R}_p)s}{K_T} + \frac{\hat{R}_t}{K_t}J_p s(\hat{L}_p + \hat{R}_p)\right)}{\hat{J}_p\hat{L}_p s^3 + (\hat{J}_p R_p + \hat{R}_e K_1)s^2 + \hat{R}_e K_2 s + \hat{R}_e K_3} \tag{8}$$

Equating coefficient of ‘s’ and solve for gains:

$$(s+\lambda_1)(s+\lambda_2)(s+\lambda_3) = \hat{J}_p s^3 + (\hat{J}_p\hat{R}_p + \hat{K}_e K_1)s^2 + \hat{K}_e K_2 s + \hat{K}_e K_3 \tag{9}$$

$$K_{T1} = \frac{\hat{J}_p \hat{L}_p(\lambda_1 + \lambda_2 + \lambda_3) - \hat{J}_p \hat{R}_p}{\hat{K}_e} \tag{10}$$

$$K_{T3} = \frac{\hat{J}_p \hat{L}_p}{\hat{K}_e}\left(\lambda_1 \lambda_2 \lambda_3\right) \tag{11}$$

$$K_{T2} = \frac{\hat{J}_p \hat{L}_p(\lambda_1 \lambda_2 + \lambda_3) - \hat{J}_p R_p\left(\lambda_1(\lambda_2 + \lambda_3) + \lambda_2 \lambda_3\right)}{\hat{K}_e} \tag{12}$$

Motion Controller:

$$(s+\lambda_{c1})(s+\lambda_{c2})(s+\lambda_{c3}) = \hat{J}_p s^3 + b_a s^2 s + K_s s + K_{is} \tag{13}$$

Current regulator:

$$(s+\lambda_i) = L_p s + R_a \tag{14}$$

Observer *estimation* frequency response functions were calculated and plotted first for ±20% estimated-inertia error then for the case of ±20% error in estimate of K_e=K_t (Figure 7). Notice first that for all cases of zero-error, both observers exactly estimate the angular velocity of motion. Overall, the Gopinath-styled observer (referred to as simply "Gopinath" for brevity) performed poorer than the Luenberger-styled observer indicating the Luenberger observer is less parameter-sensitive with respect to inertia, K_e, and K_t.

Luenberger Gains			Gopinath Gains			Motion Controller Gains			
B_o	K_{so}	K_{iso}	K_{T1}	K_{T2}	K_{T3}	B_p	K_s	K_{is}	R_a
Nm/m/s	Nm/m	Nms	rad/s Nms / A	Nm/A	Nms/A	Nm/m/s	Nm/m	Nms	V/A
24.74	7772.3	465090	0.4813	238.7	14285	12.3	1924.6	55811	21.6

Table 2. Observer Gains.

While the Luenberger observers diverge very close to the maximum tuned bandwidth (even with parameter errors), the Gopinath observer diverges at a lower bandwidth when errors are present. Since both observers contain a current-feedforward element, you will see nearly zero-lag properties out to the bandwidth of the feedback observer controller. Clearly, disturbances (in the form of modeling errors here) do not influence low frequency estimation (likely due to the addition of integrators in the observer controllers). The Gopinath observer was particularly sensitive to errors in Kt indicating its reliance on the feedforward estimation path. Notice in particular in Figure 7 that zero-lag estimation occurs even with inaccurate K_t (albeit with non-zero estimation frequency response at all frequencies).

Time-response simulations were run with *identically tuned observers* with a sample commanded trajectory (rotation angle) of θ*(t)=sin(10t). Iterations were run to establish the effects of 20% inertia underestimation and the effects of sensor noise *on command tracking accuracy*. Sensor noise was modeled as random numbers with zero-mean and unity variance.

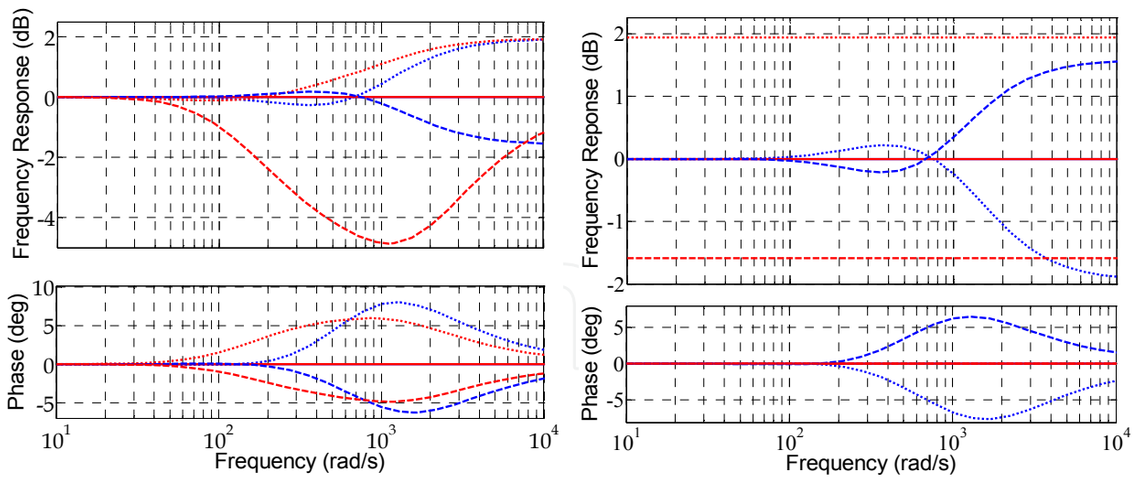

Fig. 7. LEFT: Comparison of estimation accuracy frequency response functions for incorrect $\hat{J}_p$. Luenberger (blue) Gopinath (red); dotted = -20% error, solid = 0% error; dashed = +20% error. RIGHT: Comparison of estimation accuracy frequency response functions for incorrect K_t=K_e. Luenberger (blue) Gopinath (red); dotted = -20% error, solid = 0% error; dashed = +20% error.

Figure 9 reveals the methodology for apples-to-apples comparison of effects on command tracking. Manual switches were used to evaluate a given case with the results displayed in Figure 7 and Figure 8. General conclusions may be drawn. Feedback control handles incorrectly estimated just fine, especially since inertia has nothing to do with the feedback control strategy (lacking a feedforward strategy). Using the Luenberger observer performs nearly as well if actual θ(t) is used for estimation, while it does not perform as well when θ*(t) is used for estimation. This is intuitive, since θ*(t) does not include the errors and noises associate with the process, while θ(t) includes these errors and noises. In all cases examined, the Gopinath-styled observer was inferior, which reinforces the earlier revelation of

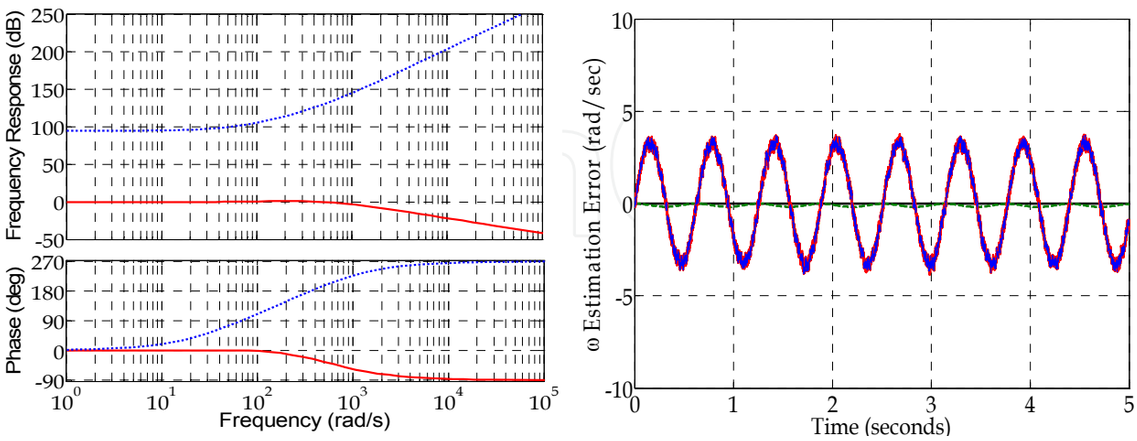

Fig. 8. LEFT: Frequency Response Functions for the motion control system. RIGHT: Estimation errors for $\hat{J}_p$ = 0.8Jp and μ=0, λ^2=1 sensor noise. Black solid line is Luenberger with θ(s) input; Green dotted line is Luenberger with θ*(s) input; red solid line is Gopinath with Ia(s) input; blue dotted line is Gopinath with I*(s) input.

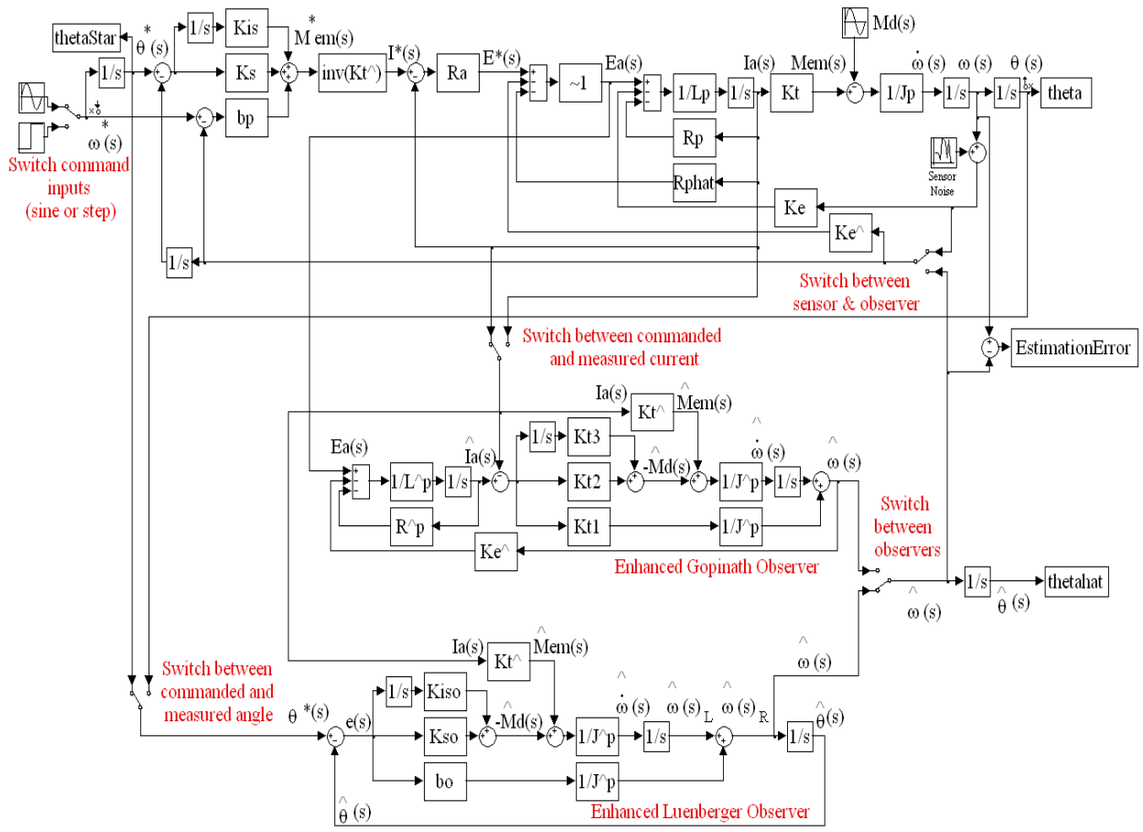

Fig. 9. SIMULINK model for error comparison Disturbance Input Decoupling (DID).

parameter sensitivity (in the discussion of the estimation frequency response functions). In addition to examining the effects on command tracking accuracy, estimation accuracy was plotted from the simulations to confirm the indications garnered from the discussion of figures 1 & 2 (estimation accuracy frequency response functions, FRFs). The single case of 20% inertia underestimation with zero-mean and unity variance sensor noise confirmed that the enhanced Luenberger-styled observer provided superior estimates compared to the Gopinath styled observer for this sinusoidal commanded trajectory.

One suggestion for improved command tracking is to remove *feedback* decoupling as done here replacing it with *feedforward* decoupling permitting the disturbance torque to excite the decoupling. One other thing: Note the maximum phase lag of 90 degrees. Such a maximum would be expected in a system with a command feedforward control scheme. Since the feedforward path would remain nearly zero-lag, the 90-degree phase lag would be creditable to Shannon's sampling-limit theory. Since there is no command feedforward control in this scheme, the lack of a maximum phase shift of 180 degrees (for a double integrator plant) is puzzling.

Observer tuning (not the current loop tuning) determines the maximum frequency for nearly zero-lag accurate estimation. Since the commanded and actual current are nearly identical (also with zero lag) out to the *higher* current loop bandwidth, *it was expected that* the effects of commanded versus actual current are mitigated by feedback decoupling (i.e. we

exceed the observer bandwidths before there is an appreciable difference in commanded versus actual current).

Actually, the Luenberger observer was sensitive to output noise associate with actual current. The noisier actual current signal does not pass through a smoothing integrator before going directly into the plant dynamics. On other hand, the Gopinath observer compares the estimated and actual/commanded current (i.e. current estimation error) through a smoothing integrator in the observer controller and also passes a portion through a separate smoothing integrator associate with angular rate estimation. Thus, the Gopinath-styled observer was insensitive to commanded versus measured current due to feedback decoupling. The Luenberger observer may be made less sensitive to the difference between commanded and actual current (and other system noises and errors) by using the actual rotation angle as input to the observer (Figure 4 and Table 2). As a matter of fact, this iteration resulted in the best performance for the evaluated case of sinusoidal sensor noise demonstrating the least mean error.

RECOMMENDATION: Use enhanced Luenberger-styled observers with actual θ(s).

6. Disturbance Input Decoupling (DID)

This paragraph reformulates the dual observer-based DID system in Yoon, 2007, consistent with physics-based control methods and furthermore evaluates opportunities in the proposed structure, [1]-[7]. Physics-based methods recommend 1) *disturbance input decoupling* followed by 2) *state feedback decoupling* of system cross-coupling, then 3) elimination of *virtual zero references*, and then finally adding *active* state feedback with full state *references*. Note the observer structure in Yoon, 2007 is different where we have added command feedforward (reference [1]) shown in Figure 6 & Figure 10. The [Yoon] paper evaluates the controlled dynamics of a magnetic levitation machine, whose dynamics are similar to a free-floating spacecraft when the cross-product has been decoupled (noting the spacecraft is suspended by gravity while the mag-lev system uses controlled magnetic field instead. Nonetheless, the physics-based decoupling principles remain the same. The main goal of DID is to formally identify the disturbance online, then use feedback to decouple the effects of disturbance input. Although the decoupling signal is actually the disturbance identified at the immediately previous timestep, using this value is far superior than simply treating disturbances as unknown quantities. The disturbance moment $M_d(s)$ is estimated in the observer in the feedforward element $\widehat{M}_{em}(s)$.

Emphasize velocity estimation for state feedback of motion controllers. The improvements achieve near-zero lag, accurate velocity estimation are displayed and zoomed in Figure 12 for clarity. The larger scale reveals the advantages over the most recently proposed improved methods. High-frequency roll-off is drastically improved by addition of command feedforward (of the true manipulated input) to the Luenberger observer. Additional inclusion of disturbance input decoupling in the motion control system improves velocity estimates in the observer, essentially eliminating roll-off and estimation lag. This later claim is more clearly displayed in the zoomed response plot in Figure 12.

The cascaded control topology should be eliminated adding full command references. Command feedforward control should be added. The electro-dynamics should not be ignored in the analysis. It causes the illusion that force is the manipulated input as opposed

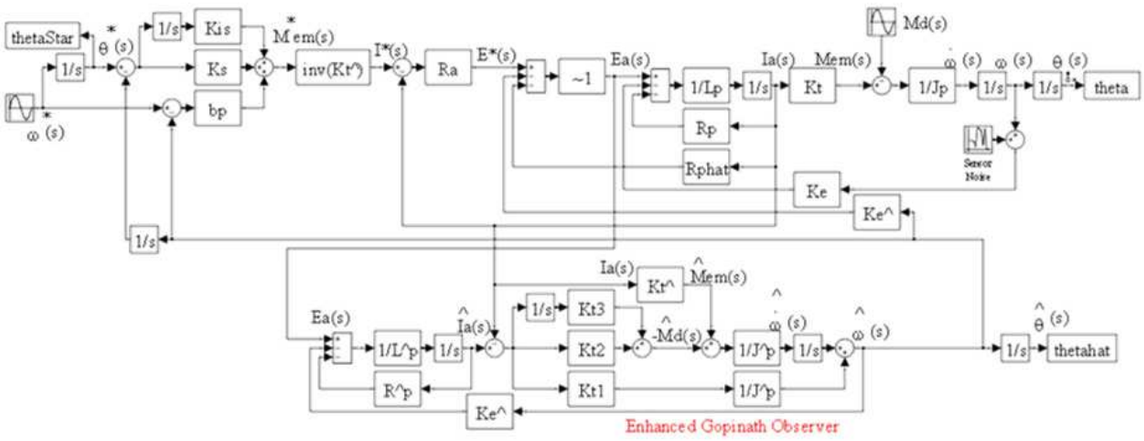

Fig. 10. Decoupled motion control w/DID & Luenberger observer with command feedforward.

to current (the true manipulated input) resulting in lower bandwidth. Neglecting the electrodynamics results in an analysis that is inadequately reinforces the experiments. Yoon refers to "disturbances forces generated by the current controller" to explain the difference between experimentation and analysis. Decoupling the electro-dynamics will improve performance even without full command references. Without manipulated input decoupling (MID), you have an implied zero-reference command for current. Assuming an inductor motor's electronics, decoupling K_e should dramatically increase disturbance rejection isolating the electrical system. The paper utilizes a dual observer to permit individual tuning for disparate purposes (DID and velocity estimation), but then implies using identical observer gains! That makes no sense. Instead of using identical gains, eliminate one of the observers to simplify the algorithmic complexity. Alternatively, utilize different gains optimized respectively for velocity and disturbance estimation. A first step for comparison requires repetition of the Yoon paper results. Equations (3), (4), and (5) in the Yoon paper are plotted in Figure 11, which should duplicate figure (5) in the Yoon paper.

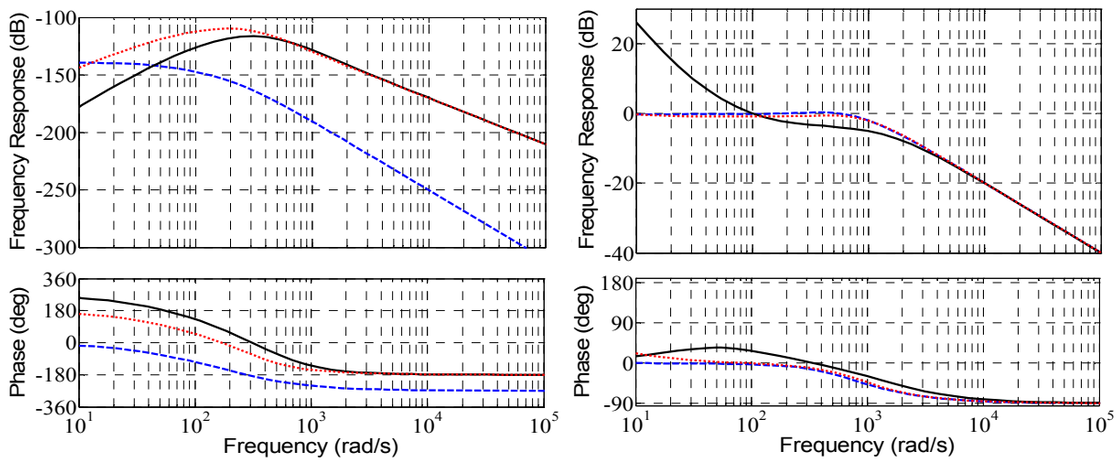

Fig. 11. LEFT: Nominal response comparison: Solid-black line is Luenberger observer; Blue-dashed line is Modified Luenberger observer; Red-dotted line is no compensation. RIGHT: Response comparison: Solid-black line is Luenberger observer; Red-dotted line is Modified Luenberger observer; Blue-dashed line is Dual Observer.

Note the slightly different result was achieved only in the case of modified observer (not the proposed dual-observer method).

Next, equations (6), (7), and (8) in Yoon, 2007 [12] were plotted in Figure 11, which duplicates Yoon's figure 6. Again, notice a slight difference this time with the estimation FRF of the basic Luenberger observer. According to the paper's plots in figure 6, the modified observer estimates more poorly than the nominal observer by dramatically overestimating velocity. This clearly indicates a labeling-error in the paper's figure. Also, the Luenberger observer does not estimate well *within the observer bandwidth*, so my results displayed here seems more credible. The difference is negligible considering the performance to be gained using physics-based reformulation.

$$F_{dist} = \left[P(s)-\hat{P}(s)\right]\left[K_d s+K_p+\frac{K_i}{s}\right] = \frac{s^2\left[\hat{P}(s)-P(s)\right]\left[K_d s+K_p+\frac{K_i}{s}\right]}{s^2} = \frac{\left[\hat{V}(s)-V(s)\right]\left[K_d s+K_p+\frac{K_i}{s}\right]}{s^2} \tag{15}$$

$$\hat{V}(s)\left[1+\frac{L_d}{\hat{M}}\frac{1}{s}+\frac{L_p}{\hat{M}}\frac{1}{s^2}+\frac{L_i}{\hat{M}}\frac{1}{s^3}\right] = V(s)\left[\frac{\hat{K}_T}{K_T}\frac{M}{\hat{M}}+\frac{L_d}{\hat{M}}\frac{1}{s}+\frac{L_p}{\hat{M}}\frac{1}{s^2}+\frac{L_i}{\hat{M}}\frac{1}{s^3}\right]+ +\left[\hat{V}(s)-V(s)\right]\left[K_d+\frac{K_p}{s}+\frac{K_i}{s^2}\right] \tag{16}$$

$$\hat{V}(s)\left[1+\frac{L_d}{\hat{M}}\frac{1}{s}+\frac{L_p}{\hat{M}}\frac{1}{s^2}+\frac{L_i}{\hat{M}}\frac{1}{s^3}-K_d-\frac{K_p}{s}-\frac{K_i}{s^2}\right] = =V(s)\left[\frac{\hat{K}_T}{K_T}\frac{M}{\hat{M}}+\frac{L_d}{\hat{M}}\frac{1}{s}+\frac{L_p}{\hat{M}}\frac{1}{s^2}+\frac{L_i}{\hat{M}}\frac{1}{s^3}-K_d-\frac{K_p}{s}-\frac{K_i}{s^2}\right] \tag{17}$$

Multiplying by s^3:

$$\hat{V}(s)\left[s^3+\frac{L_d}{\hat{M}}s^2+\frac{L_p}{\hat{M}}s+\frac{L_i}{\hat{M}}-K_d s^3-K_p s^2-K_i s\right] = =V(s)\left[\frac{\hat{K}_T}{K_T}\frac{M}{\hat{M}}s^3+\frac{L_d}{\hat{M}}s^2+\frac{L_p}{\hat{M}}s+\frac{L_i}{\hat{M}}-K_d s^3-K_p s^2-K_i s\right] \tag{18}$$

$$\frac{\hat{V}(s)}{V(s)} = \frac{\left[\frac{\hat{K}_T}{K_T}\frac{M}{\hat{M}}-K_d\right]s^3+\left[\frac{L_d}{\hat{M}}-K_p\right]s^2+\left[\frac{L_p}{\hat{M}}-K_i\right]s+\frac{L_i}{\hat{M}}}{\left[1-K_d\right]s^3+\left[\frac{L_d}{\hat{M}}-K_p\right]s^2+\left[\frac{L_p}{\hat{M}}-K_i\right]s+\frac{L_i}{\hat{M}}} \tag{19}$$

The reformulation (Figure 10) results in the estimation FRF *with DID and command feedforward* is displayed Figure 12. Immediately notice that addition of the command feedforward to the modified Luenberger observer yields *nearly-zero* lag estimates, far superior to Yoon, 2007 (which omitted the command feedforward path in what they call an observer). It is a premise of the physics-based methodology that the title "observer" implies nearly-zero lag estimation, so one might argue that the Yoon paper really utilizes a state filter rather than a state observer.

The results using the physics-based methodology are clearly superior despite relative algorithmic simplicity. Adding the command feedforward permits accurate, near-zero lag estimation of velocity without a velocity sensor. Furthermore, disturbance input decoupling increases system robustness and permits accurate estimation inaccuracy even when unknown disturbances are present. Certainly, accounting for the electrodynamics should always be done rather than neglecting them as "system noise" as done in Yoon, 2007.

Figure 12 displays a Solid-blue line is Modified Luenberger observer with command feedforward; Red-dashed line is Modified Luenberger observer with command feedforward and disturbance input decoupling. RIGHT: Observer Improvements estimation comparison: Dotted-black line from the Yoon paper (using dual observers). Solid-blue line is Modified Luenberger observer with command feedforward; Red-dashed line is Modified Luenberger observer with command feedforward and disturbance input decoupling; Dashed-black line is Dual Observers.

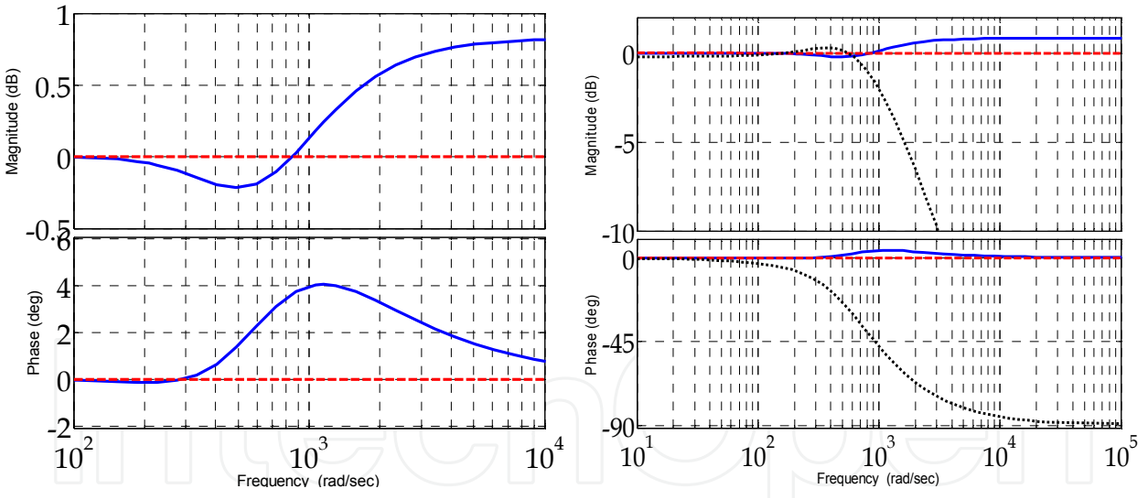

Fig. 12. LEFT: Observer Improvements estimation comparison.

7. Physics-based methods for idealized feedforward control

Feedforward control is a basic starting point for spacecraft rotational maneuver control. Assuming a rigid body spacecraft model in the presence of no disturbances and known inertia [J], an open loop (essentially feedforward) command should exactly accomplish the commanded maneuver. When disturbances are present, feedback is typically utilized to insure command tracking. Additionally, if the spacecraft inertia [J] is unknown, the open command will not yield tracking. Consider a spacecraft that is actually much heavier about

it's yaw axis than anticipated in the assumed model. The same open loop command torque would yield less rotational motion for heavier spacecraft. Similarly, if the spacecraft were much lighter than modeled, the open loop command torque would result in excess rotation of the lighter spacecraft. Observe in Figure 13, a rigid spacecraft simulator (TASS2 at Naval Postgraduate School) has been modeled in SIMULINK. An open loop feedforward command has been formulated to produce 10 seconds of regulation followed by a 30° yaw-only rotation in 10 seconds, followed by another 10 seconds of regulation at the new attitude. The assumed inertia matrix is not diagonal, so coupled dynamics are accounted for in the feedforward command.

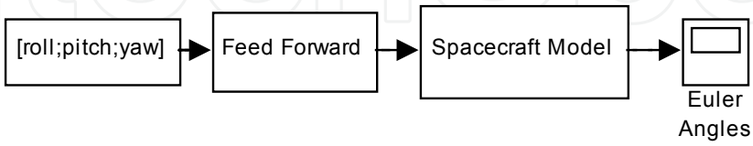

Fig. 13. SIMULINK model of TASS2 Spacecraft Simulator at Naval Postgraduate School.

With no disturbances and a known, correct model, the open loop feedforward command can effectively perform the maneuver.

$$[\mathbf{J}]_{\text{modeled}} = [\mathbf{J}]_{\text{previously estimated}} = [\mathbf{J}]_{\text{feedforward}} = \begin{bmatrix} 119.1259 & -15.7678 & -6.5486 \\ -15.7678 & 150.6615 & 22.3164 \\ -6.5486 & 22.3164 & 106.0288 \end{bmatrix} \quad (20)$$

Recall in the real world systems are not always as we model them, disturbances are presence, and our sensor measurements of the maneuver will also be quite noisy. Nonetheless, the idealized case is a useful place to start, as it gives us confidence that our model has been correctly coded. Proof is easily provided by sending an acceleration command (scaled by the inertia) to the spacecraft model to verify the identical acceleration is produced (Figure 14). We have not yet added noise, disturbances, or modeling errors, so exact following should be anticipated. Next, we will alter the inertia [J] of TASS2. This is real-world, since the spacecraft has recently received its optical payload, so the yaw inertia

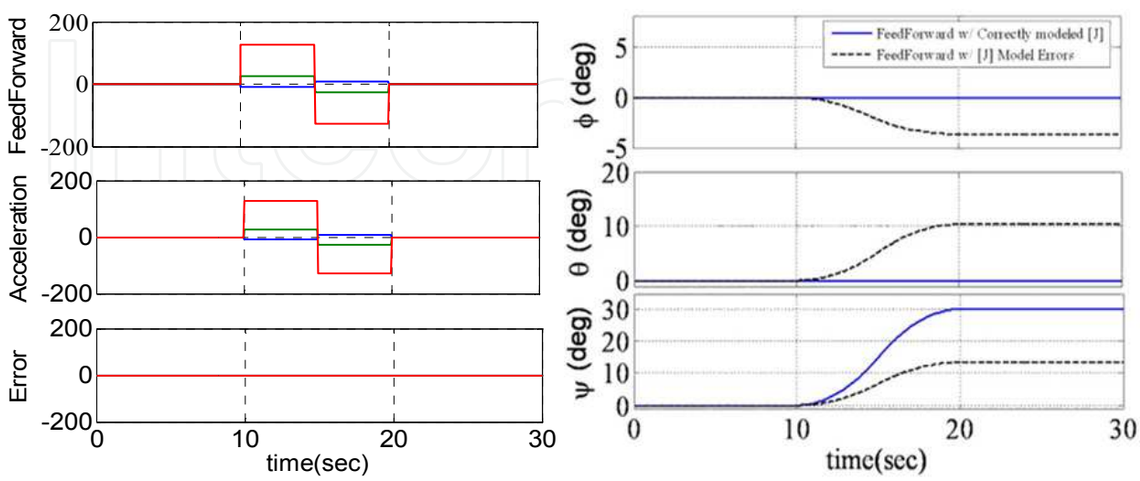

Fig. 14. LEFT: Feedforward input and resultant TASS2 acceleration (note zero error). RIGHT: Open Loop Feedforward TASS2 Maneuver Simulation.

components have increased significantly. Using the previous experimentally determined inertia [J] in the feedforward command should result in difficulties meeting the open loop pointing command.

Notice in Figure 14 the maneuver is not correctly executed using the identical feedforward command for the assumed, modeled TASS2. The current inertia matrix has not been experimentally determined, so inertia components were varied arbitrarily (making sure to increase yaw inertia dramatically). This new inertia was used in the spacecraft model, but is presumed to be unknown. Thus, the previous modeled open loop feedforward command is used and proven to ineffective. Options to improve system performance include feedback, and adapting the feedforward command to eliminate the tracking error. Since adaptive control is more difficult, we will first examine feedback control with the identical models and maneuver.

8. Feedback control

Feedback control components multiply a gain to the tracking error components in each of the 3-axes. When multiplying gains to the tracking error itself, the control is referred to as proportional control (or P-control). When multiplying gains to the tracking error integral, the control is referred to as integral control (or I-control). Finally, when multiplying gains to the tracking error rate (derivative), the control is referred to as derivative control (or D-control). Summing multiple gained control signals results in combinations such as: PI, PD, PID, etc. PD control is extremely common for Hamiltonian systems, as it is easily veritably a stable control. PD control was augmented to the previous case of feedforward control with inertia modeling errors (Figure 15) dramatically improving performance, while not restoring the ideal case.

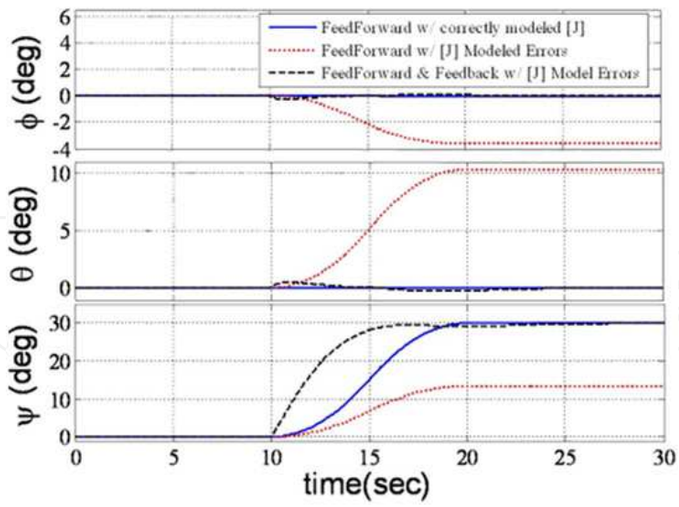

Fig. 15. Demonstration of Feedback Control Effectiveness.

It is clear that feedback control augmentation is a powerful tool to eliminate real world factors like modeling errors. An identical comparison was performed with gravity gradient disturbances associated with an unbalanced TASS2. The comparison is not presented here for brevity's sake, but the results were qualitatively identical.

While feedback appears extremely effective to accomplish the overall tracking maneuver, some missions require faster, more accurate tracking with less error. Such missions often consider augmenting the feedforward-feedback control scheme by adding adaptive control to either signal.

9. Adaptive control

Adaptive control techniques typically adapt control inputs based upon errors tracking commanded trajectories and/or estimation errors. *Direct* adaptive control techniques typically directly adapt the control signal to eliminate tracking errors without estimation of unknown system parameters. *Indirect* adaptive control techniques indirectly adapt the control signal by modifying estimates of unknown system parameters. The adaptation rule is derived using a proof that demonstrates the rapid elimination of tracking errors (the real objective). The proof must also demonstrate stability, since the closed loop system is highly nonlinear with the adaptive control included. Two fields of application of adaptive control is robotic manipulators and spacecraft maneuvers utilizing both approaches [15], [16], [17].

While some adaptive techniques concentrate on adaptation of the feedback control, others have been suggested to modify a feedforward control command retaining a typical feedback controller, such as Proportional-Derivative (PD). Adaptation of the feedforward signal has been suggested in the inertial reference frame [18], [19], but the resulting regression model requires several pages to express for 3-dimensional spacecraft rotational maneuvers. The regression matrix of "knowns" is required in the control calculation, so this approach is computationally inappropriate for spacecraft rotational maneuvers. Subsequently, the identical approach was suggested for implementation in the body reference frame [20]. The method was demonstrated for slip translation of the space shuttle. This method appears promising for practical utilization in 3-dimensional spacecraft rotational maneuvers. A derivation of the Slotine-Fossen approach is derived for 3-dimensional spacecraft rotational maneuvers next, then implementation permits evaluation of the effectiveness of the approach in the context of the previous results for classical feedforward-feedback control of the TASS2 plant with modeling errors.

9.1 Adaptive feedforward command derivation

The equation of motion may be written by various methods (Newton-Euler, Lagrange, Kane's, momentum, etc.) as follows: $[\mathbf{J}]\{\ddot{\mathrm{q}}\}_B + [\mathbf{C}]\{\dot{\mathrm{q}}\}_B = \{\tau\}_B$ where $[\mathbf{J}]$ is the inertia matrix, $[\mathbf{C}]$ is the Coriolis matrix representing the cross-coupling dynamics, $\boldsymbol{\tau}$ is the sum of external torques and q is the body coordinates (quaternion, Euler angles, etc.). The body coordinates may be transformed to inertial coordinates via the transformation matrix $[\mathbf{S}]$ per the following: $\{\dot{\mathrm{x}}\}_i = [\mathbf{S}]_{B2i}\{\dot{\mathrm{q}}\}_B$. Similarly, we may define a reference trajectory *in the body coordinates*: $\{\dot{\mathrm{x}}_\mathrm{r}\}_i = [\mathbf{S}]_{B2i}\{\dot{\mathrm{q}}_\mathrm{r}\}_B$. Rewriting the transformation and differentiating:

$\{\dot{\mathrm{q}}_\mathrm{r}\}_B = [\mathbf{S}]^{-1}\{\dot{\mathrm{x}}_\mathrm{r}\}_i \rightarrow \{\ddot{q}_r\}_B = [\mathbf{S}]^{-1}\{\ddot{x}_r\}_i - [\mathbf{S}]^{-1}[\dot{\mathbf{S}}][\mathbf{S}]^{-1}\{\dot{\mathrm{x}}_\mathrm{r}\}_i$. This may be substitute into the equation of motion allowing us to express the equation of motion in terms of the reference trajectory.

$$[\mathbf{J}]\left[[\mathbf{S}]^{-1}\{\ddot{x}_r\}_i - [\mathbf{S}]^{-1}[\dot{\mathbf{S}}][\mathbf{S}]^{-1}\{\dot{x}_r\}_i\right] + [\mathbf{C}]\left[[\mathbf{S}]^{-1}\{\ddot{x}_r\}_i\right] = \{\tau\}_B \tag{21}$$

$$[\mathbf{J}][\mathbf{S}]^{-1}\{\ddot{x}_r\}_i + \left[-[\mathbf{J}][\mathbf{S}]^{-1}[\dot{\mathbf{S}}][\mathbf{S}]^{-1} + [\mathbf{C}][\mathbf{S}]^{-1}\right]\{\dot{x}_r\}_i = \{\tau\}_B \tag{22}$$

Pre-multiplying by $[\mathbf{S}]^T[\mathbf{S}]^{-T} = 1$ allows us to understand [Slotine]'s original approach in reference [19]:

$$[\mathbf{S}]^T[\mathbf{S}]^{-T}[\mathbf{J}][\mathbf{S}]^{-1}\{\ddot{x}_r\}_i + [\mathbf{S}]^T[\mathbf{S}]^{-T}\left[-[\mathbf{J}][\mathbf{S}]^{-1}[\dot{\mathbf{S}}][\mathbf{S}]^{-1} + [\mathbf{C}][\mathbf{S}]^{-1}\right]\{\dot{x}_r\}_i = [\mathbf{S}]^T[\mathbf{S}]^{-T}\{\tau\}_B \quad (23)$$

$$[\mathbf{S}]^T\underbrace{[\mathbf{S}]^{-T}[\mathbf{J}][\mathbf{S}]^{-1}}_{Slotine's\ J^*}\{\ddot{x}_r\}_i + [\mathbf{S}]^T\underbrace{\left[-[\mathbf{S}]^{-T}[\mathbf{J}][\mathbf{S}]^{-1}[\dot{\mathbf{S}}][\mathbf{S}]^{-1} + [\mathbf{S}]^{-T}[\mathbf{C}][\mathbf{S}]^{-1}\right]}_{Slotine's\ C^*}\{\dot{x}_r\}_i = [\mathbf{S}]^T[\mathbf{S}]^{-T}\{\tau\}_B \quad (24)$$

$$[\mathbf{S}]^T\left[\mathbf{J}^*\right]\{\ddot{x}_r\}_i + [\mathbf{S}]^T\left[\mathbf{C}^*\right]\{\dot{x}_r\}_i = [\mathbf{S}]^T\underbrace{\left[\mathbf{J}^*\right]\{\ddot{x}_r\}_i + \left[\mathbf{C}^*\right]\{\dot{x}_r\}_i}_{\Phi^*(x,\dot{x},\ddot{x}_r,\dot{x}_r)\theta} = \{\tau\}_B \quad (25)$$

Slotine uses the linear regression model to define an equivalent system based on parameter estimates:

$$\Phi^*(\mathrm{x},\dot{\mathrm{x}},\dot{\mathrm{x}}_\mathrm{r},\ddot{\mathrm{x}}_\mathrm{r})\Theta = \underbrace{\Phi^*(\mathrm{x},\dot{\mathrm{x}},\dot{\mathrm{x}}_\mathrm{r},\ddot{\mathrm{x}}_\mathrm{r})}_{\text{knowns}}\ \underbrace{\widehat{\Theta}}_{\text{unknowns}} + \text{error}. \quad (26)$$

The estimates $\widehat{\Theta}$are adapted using an adaption rule that makes the closed loop system stable. The regression model is then used in the control, which is where the complication arises. The $\Phi^*(\mathrm{x},\dot{\mathrm{x}},\dot{\mathrm{x}}_\mathrm{r},\ddot{\mathrm{x}}_\mathrm{r})$ matrix of "knowns" occupies several pages and is used *at each time* step to formulate the adapted control signal making the method computationally impractical. [Fossen] on the other hand formulates the regression model in the body coordinates eliminated the complications seen above with the numerous multiplications with the coordinate transformation matrix [**S**]. Picking up from [Slotine]'s method above, we can simply express the regression model *including* the transformation matrix:

$$[\mathbf{S}]^T\left[\mathbf{J}^*\right]\{\ddot{x}_r\}_i + [\mathbf{S}]^T\left[\mathbf{C}^*\right]\{\dot{x}_r\}_i = \underbrace{[\mathbf{S}]^T\left[\left[\mathbf{J}^*\right]\{\ddot{x}_r\}_i + \left[\mathbf{C}^*\right]\{\dot{x}_r\}_i\right]}_{\Phi(x,\dot{q},\dot{q}_r,\ddot{q}_r)\theta} = \{\tau\}_B \quad (27)$$

noting the$\Phi(\mathrm{x},\dot{\mathrm{x}},\dot{\mathrm{x}}_\mathrm{r},\ddot{\mathrm{x}}_\mathrm{r})$ matrix of "knowns" has no asterisk. Preface [Slotine]'s mathematical trick (pre-multiplication) above:

$$[\mathbf{J}][\mathbf{S}]^{-1}\{\ddot{x}_r\}_i + \left[-[\mathbf{J}][\mathbf{S}]^{-1}[\dot{\mathbf{S}}][\mathbf{S}]^{-1} + [\mathbf{C}][\mathbf{S}]^{-1}\right]\{\dot{x}_r\}_i = \{\tau\}_B\ . \quad (28)$$

Continuing here yields [Fossen]'s substantial simplification through the following 3 steps: Solve the earlier defined transformation equations for $\dot{\mathrm{x}}_\mathrm{r}$ & $\ddot{\mathrm{x}}_\mathrm{r}$:

$$\{\dot{x}_r\} = [\mathbf{S}]\{\dot{q}_r\} \quad (29)$$

$$\{\ddot{x}_r\}_i = [\mathbf{S}]\left[\ddot{q}_r + [\mathbf{S}]^{-1}[\dot{\mathbf{S}}][\mathbf{S}]^{-1}\{\dot{x}_r\}\right] = [\mathbf{S}]\ddot{q}_r + [\dot{\mathbf{S}}][\mathbf{S}]^{-1}[\mathbf{S}]\{\dot{q}_r\} = [\mathbf{S}]\ddot{q}_r + [\dot{\mathbf{S}}]\{\dot{q}_r\} \quad (30)$$

Substitute into $[\mathbf{J}][\mathbf{S}]^{-1}\{\ddot{x}_r\}_i + \left[-[\mathbf{J}][\mathbf{S}]^{-1}[\dot{\mathbf{S}}][\mathbf{S}]^{-1} + [\mathbf{C}][\mathbf{S}]^{-1}\right]\{\dot{x}_r\}_i = \{\tau\}_B$ instead of pre-multiplying.

$$[\mathbf{J}][\mathbf{S}]^{-1}\underbrace{\left[[\mathbf{S}]\ddot{q}_r + [\dot{\mathbf{S}}]\{\dot{q}_r\}\right]}_{\{\ddot{x}_r\}_i} + \left[-[\mathbf{J}][\mathbf{S}]^{-1}[\dot{\mathbf{S}}][\mathbf{S}]^{-1} + [\mathbf{C}][\mathbf{S}]^{-1}\right]\underbrace{[\mathbf{S}]\{\dot{q}_r\}}_{\{\dot{x}_r\}_i} = \{\tau\}_B \quad (31)$$

Reduce this to linear regression form:

$$[\mathbf{J}][\mathbf{S}]^{-1}[\mathbf{S}]\ddot{q}_r + [\mathbf{J}][\mathbf{S}]^{-1}[\dot{\mathbf{S}}]\{\dot{q}_r\} - [\mathbf{J}][\mathbf{S}]^{-1}[\dot{\mathbf{S}}][\mathbf{S}]^{-1}[\mathbf{S}]\{\dot{q}_r\} + [\mathbf{C}][\mathbf{S}]^{-1}[\mathbf{S}]\{\dot{q}_r\} = \{\tau\}_B \tag{32}$$

$$[\mathbf{J}]\ddot{q}_r + \left[\cancel{[\mathbf{J}][\mathbf{S}]^{-1}[\dot{\mathbf{S}}] - [\mathbf{J}][\mathbf{S}]^{-1}[\dot{\mathbf{S}}]}^{0} + [\mathbf{C}] \right]\{\dot{q}_r\} = \{\tau\}_B \tag{33}$$

$$\boxed{[\mathbf{J}]\{\ddot{q}_r\} + [\mathbf{C}]\{\dot{q}_r\} = \{\tau\}_B} \tag{34}$$

All that remains now is to multiply this out long-hand and regroup the terms into the linear regression model: $\Phi^*(\mathrm{x}, \dot{\mathrm{x}}, \dot{\mathrm{x}}_\mathrm{r}, \ddot{\mathrm{x}}_\mathrm{r})\Theta = \underbrace{\Phi^*(\mathrm{x}, \dot{\mathrm{x}}, \dot{\mathrm{x}}_\mathrm{r}, \ddot{\mathrm{x}}_\mathrm{r})}_{\text{knowns}} \underbrace{\widehat{\Theta}}_{\text{unknowns}} + \text{error}$. In order to do this, we must define the reference trajectory. The modifications to the overall feedforward control strategy may be embodied in these two venues: 1) estimate/adapt estimates of inertia in the regression model above, and 2) choose a reference trajectory that addresses system lead/lag when applying the assumed control to a spacecraft with modeling errors, disturbances and noise.

9.2 Reference trajectory

Define the reference trajectory such that the control helps the spacecraft "catch up" to the commanded trajectory. If the spacecraft is actually heavier than modeled, it needs a little extra control to achieve tracking than will be provided by classical feedforward control. If the spacecraft is actually lighter than modeled, the control must be reduced so as not to overshoot the commanded trajectory. Consider defining the reference trajectory as follows:

$$\ddot{q}_r = \ddot{q}_d - \lambda(\dot{q} - \dot{q}_d) \text{ and } \dot{q}_r = \dot{q}_d - \lambda(q - q_d) \tag{35}$$

Note we have scaled the reference acceleration and velocity to add/subtract the velocity and position error respectively scaled by a positive definite constant, λ. This should help the feedforward control component regardless of indirect adaption. Accordingly, subsequent sections will evaluate the effectiveness of the reference trajectory by itself and the also the indirect adaption/estimation by itself as well. First, let's conclude the derivation by multiplying out the linear regression form so that the reader can have the simple equation for spacecraft rotational maneuvers.

9.3 Feedforward & feedback control with reference trajectories

Simplify $[\mathbf{J}]\{\ddot{q}_r\} + [\mathbf{C}]\{\dot{q}_r\} = \{\tau\}_B$ letting $\ddot{q}_r = \ddot{q}_d - \lambda(\dot{q} - \dot{q}_d)$ and $\dot{q}_r = \dot{q}_d - \lambda(q - q_d)$ and use $\ddot{\mathrm{q}}_\mathrm{r} = \ddot{\omega}_\mathrm{r}$ and $\dot{\mathrm{q}}_\mathrm{r} = \dot{\omega}_\mathrm{r}$:

$[\mathbf{J}]\{\dot{\omega}_r\} + [\mathbf{C}]\{\omega_r\} = \{\tau\}_B$

$[\mathbf{J}]\{\dot{\omega}_r\} = [\mathbf{J}]\{\omega_r\} \times \{\omega_r\} + \{\tau\}_B$

$[\mathbf{J}]\{\dot{\omega}_r\} = [\mathbf{H}\times]\{\omega_r\} + \{\tau\}_B$ where $[\mathbf{H}\times]$ is the skew symmetric matrix form of the momentum vector. Expand $[\mathrm{J}]\{\dot{\omega}_\mathrm{r}\} - [\mathrm{H}\times] = \{\tau\}_\mathrm{B}$:

$$\begin{bmatrix} J_{xx} & J_{xy} & J_{xz} \\ J_{yx} & J_{yy} & J_{yz} \\ J_{zx} & J_{zy} & J_{zz} \end{bmatrix} \begin{Bmatrix} \dot{\omega}_x \\ \dot{\omega}_y \\ \dot{\omega}_z \end{Bmatrix} - \begin{bmatrix} 0 & -H_z & H_y \\ H_z & 0 & -H_x \\ -H_y & H_x & 0 \end{bmatrix} \begin{Bmatrix} \omega_x \\ \omega_y \\ \omega_z \end{Bmatrix} = \begin{Bmatrix} \tau_x \\ \tau_y \\ \tau_z \end{Bmatrix}_B = \tag{36}$$

$$= \underbrace{\left[\hat{\mathbf{J}}\right]\{\dot{\omega}_r\} - \left[\hat{\mathbf{H}}\times\right]\{\omega_r\}}_{\text{Adaptive Feedforward}} - \underbrace{K_d S^{-1}(\dot{x} - \dot{x}_r)}_{\text{Ref Trajectory Feedback}}$$

$$\begin{bmatrix} -H_y\omega_z + H_z\omega_y + J_{xx}\dot{\omega}_x + J_{xy}\dot{\omega}_y + J_{xz}\dot{\omega}_z \\ H_x\omega_z - H_z\omega_x + J_{yx}\dot{\omega}_x + J_{yy}\dot{\omega}_y + J_{yz}\dot{\omega}_z \\ -H_x\omega_y + H_y\omega_x + J_{zx}\dot{\omega}_x + J_{zy}\dot{\omega}_y + J_{zz}\dot{\omega}_z \end{bmatrix} = \begin{Bmatrix} \tau_x \\ \tau_y \\ \tau_z \end{Bmatrix}_B \tag{37}$$

Let $\theta^T = \{J_{xx} \;\; J_{xy} \;\; J_{xz} \;\; J_{yy} \;\; J_{yz} \;\; J_{zz} \;\; H_x \;\; H_y \;\; H_z\}$ and assume $J_{xy} = J_{yx}, J_{xz} = J_{zx}, J_{yz} = J_{zy}$ allowing us to express $\left[\Phi(\dot{\omega},\ddot{\omega})\right]_{3x9}\{\theta\}_{9x1}$:

$$\begin{bmatrix} \dot{\omega}_x & \dot{\omega}_y & \dot{\omega}_z & 0 & 0 & 0 & 0 & -\omega_z & \omega_y \\ 0 & \dot{\omega}_x & 0 & \dot{\omega}_y & \dot{\omega}_z & 0 & \omega_z & 0 & \omega_x \\ 0 & 0 & \dot{\omega}_x & 0 & \dot{\omega}_y & \dot{\omega}_z & -\omega_y & \omega_x & 0 \end{bmatrix} \begin{Bmatrix} J_{xx} \\ J_{xy} \\ J_{xz} \\ J_{yy} \\ J_{yz} \\ J_{zz} \\ H_x \\ H_y \\ H_z \end{Bmatrix} = \left[\Phi(\dot{\omega},\ddot{\omega})\right]_{3x9}\{\theta\}_{9x1} = \left[\hat{\Phi}\right]\{\theta\} + error$$

$$\{\tau\} = \left[\hat{\Phi}\right]\{\theta\} - K_d S^{-1}(\dot{x} - \dot{x}_r) \;\leftarrow \boxed{\text{Use this control}} \tag{38}$$

$$\text{Where } \left\{\dot{\hat{\theta}}\right\} = -\Gamma[\Phi]_{[3x9]}[S]^{-1}(\dot{x} - \dot{x}_r) = -\Gamma[\Phi]_{[3x9]}(\dot{q} - \dot{q}_r) \;\leftarrow \boxed{\text{use this adaption rule}} \tag{39}$$

9.4 Adaptive feedforward effectiveness

Especially since typical feedback control deals with modeling errors effectively, we wish to evaluate the effectiveness of indirect adaptive feedforward control with a rigorously disciplined approach. Accordingly, the examination will evaluate the individual effectiveness of each control component in the following paragraphs:

- Reference trajectory without indirect adaption (feedforward, feedback, and both)
- Indirect adaption without a scaled reference trajectory (feedforward, feedback, and both)
- Indirect adaption with reference trajectory (previously derived application of [Fossen] suggested improvement to [Slotine]'s method)

The examination is performed by manually activating switches in the SIMULINK simulation model to insure all aspects of the maneuver are identical with exception of the aspect being switched for investigation. Note the feedback control is configured as a proportional-derivative-integral (PID) controller with the following gains: K_p=100, K_d=300, K_I=0, thus a PD controller.

It seems likely that utilization of the reference trajectory alone should improve system performance without the computational complications of estimation/adaption. Consider the reference trajectory as derived previously: $\ddot{q}_r = \ddot{q}_d - \lambda(\dot{q} - \dot{q}_d)$ and $\dot{q}_r = \dot{q}_d - \lambda(q - q_d)$. This trajectory adds/subtracts a little extra amount (the previous integral scaled by a positive constant). If the system is lagging behind the desired angle for example, that lag is scaled and added to the reference velocity trajectory resulting in more control inputs. Since we use measurements to generate the reference command, it seems intuitively appropriate for feedback control. Nonetheless, it is implemented in feedforward, feedback, and both for completeness sake.

Referencing Figure 16, note that the reference trajectory with feedforward control *only* with a correctly modeled system is not effective. This makes sense, since the feedforward control on a correctly modeled plant with no disturbances was previously demonstrated to perform well (Figure 14) while unrealistic for real world systems.

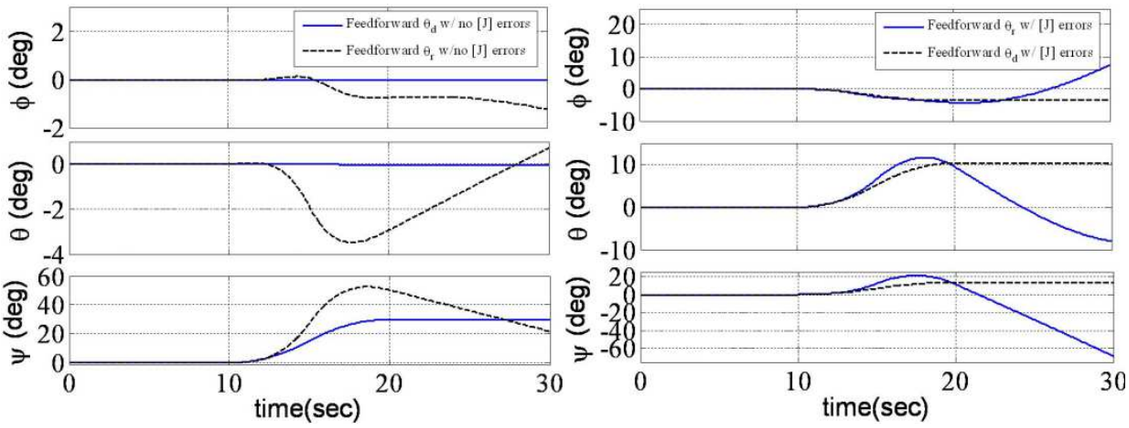

Fig. 16. LEFT: Feedforward (only) control with correctly modeled inertia. RIGHT: Feedforward (only) control with inertia errors.

Next, consider the reference trajectory for a system that is not well modeled. As we saw previously (Figure 15), open loop control when the inertia is increased results in the system falling short of the desired maneuver. The control is designed for a lighter spacecraft. We see in Figure 16 that feedforward control alone with a reference trajectory fairs no better. As a matter of fact, the performance is worse. Addition of feedback control seems appropriate. Before examining feedback control added to feedforward control, first examine feedback control by itself so that we may see the effects of the reference trajectory. Notice in Figure 17 that when the model is well known (correct), feedback control works quite well, and system performance is dramatically improved using the reference trajectory. Again, this is intuitive since the control is given a little something extra to account for tracking errors. This is also important for us to remember when analyzing indirect adaptive control with a reference trajectory. Tracking performance can be improved considerably without the complications of inertia estimation/adaption if the system is the assumed model.

When the model is not known, or has changed considerably from its assumed form, the performance improvement using the reference trajectory is not as pronounced as just seen

with a well known model. Figure 17 illustrates that system damping has been reduced by the addition of the reference trajectory. The initial response is much faster, but there is overshoot and oscillatory settling. Notice in this example the two plots settle in similar times, so use of the reference trajectory has not drastically improved or degraded system performance.

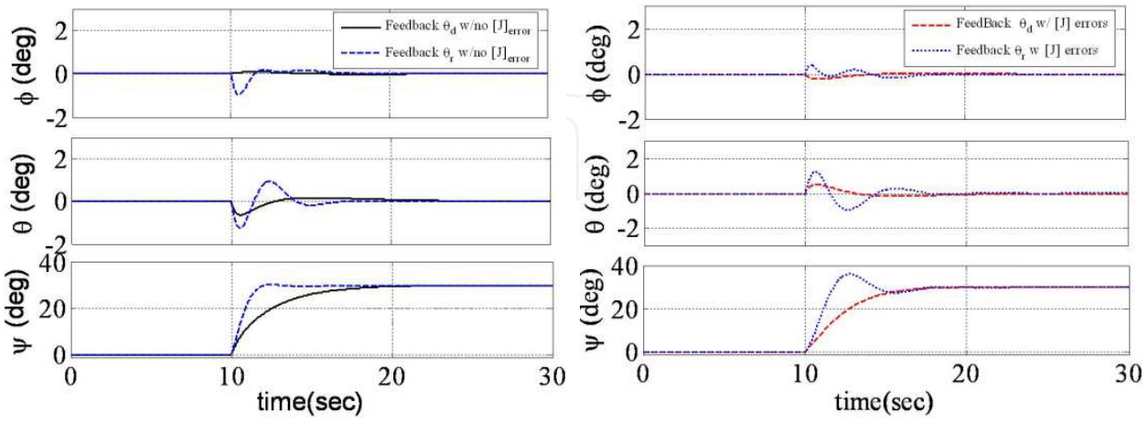

Fig. 17. LEFT: Feedback (only) control with correctly modeled inertia. RIGHT: Feedback (only) control with inertia errors.

Thus far, we see that the reference trajectory does not improve system performance when using feedforward control alone, but can improve performance with feedback control alone especially when the system inertia is known. Next, consider combined feedback & feedforward control. Figure 18 reveals expected results. Feedforward and feedback control with a reference trajectory is superior to using the desired trajectory when the plant model is known (no inertia errors). Similarly to the previous results, the reference trajectory with high inertia errors reduces system damping and exhibits faster response with overshoot and oscillatory settling. To conclude the evaluation of control with the reference trajectory without adaption/estimation, consider using the reference trajectory for feedback only and maintain the desired trajectory to formulate the feedforward control.

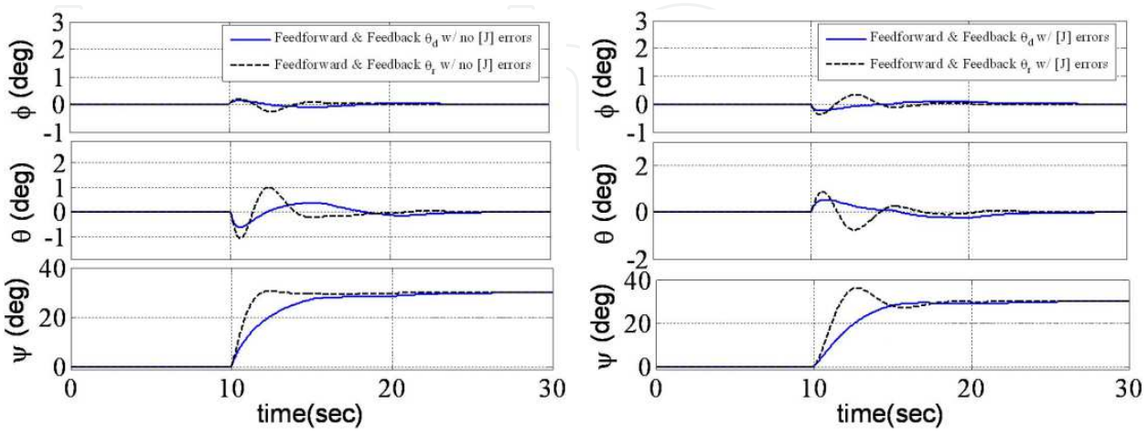

Fig. 18. LEFT: Feedforward & Feedback control with correctly modeled inertia. RIGHT: Feedforward & feedback control with inertia errors.

Notice in Figure 18 the system performance using the reference signal for both feedback and feedforward. This leaves us with a good understanding of how the reference trajectory affects the controlled system. To generalize:

Feedback control may be improved by utilization of a reference trajectory that adds a component scaled on the previous integral tracking error. When the system model is known, performance is improved drastically. In the example, J_{zz} was altered >100% and the reference trajectory still effectively controlled the spacecraft yaw maneuver.

Such reference trajectories are not advisable for feedforward control. Use of the reference trajectory in feedforward control does not improve system performance even in combination with feedback control.

Now that we have a good understanding that reference trajectories can improve system performance without estimation/adaption, let's continue by examining indirect adaptive control without the reference trajectory.

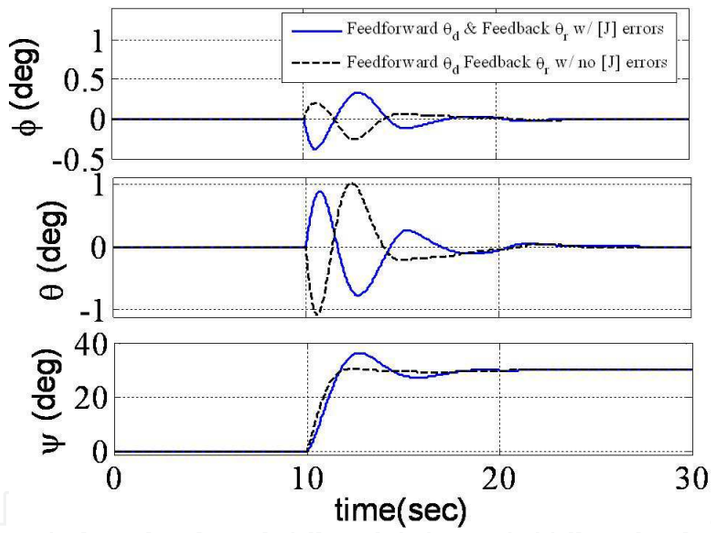

Fig. 19. Feedforward θ_d & Feedback θ_r with and without inertia errors.

9.5 Adaption without reference trajectory

Figure 20 displays a comparison of indirect adaptive control with and without a reference trajectory. In both cases, estimates are used to update a feedforward signal. The former case feeds the reference signal is generated by adding the scaled previous integral (scaled by a positive constant λ) as previously discussed. The latter case sets $\lambda=0$ making the reference trajectory equal to the desired (commanded) trajectory. The figure reveals that adaption//estimation alone does not produce good control. The reference trajectory is a key piece of the control scheme's effectiveness. This is intuitive having established the significance of the reference trajectory in previous sections of this study.

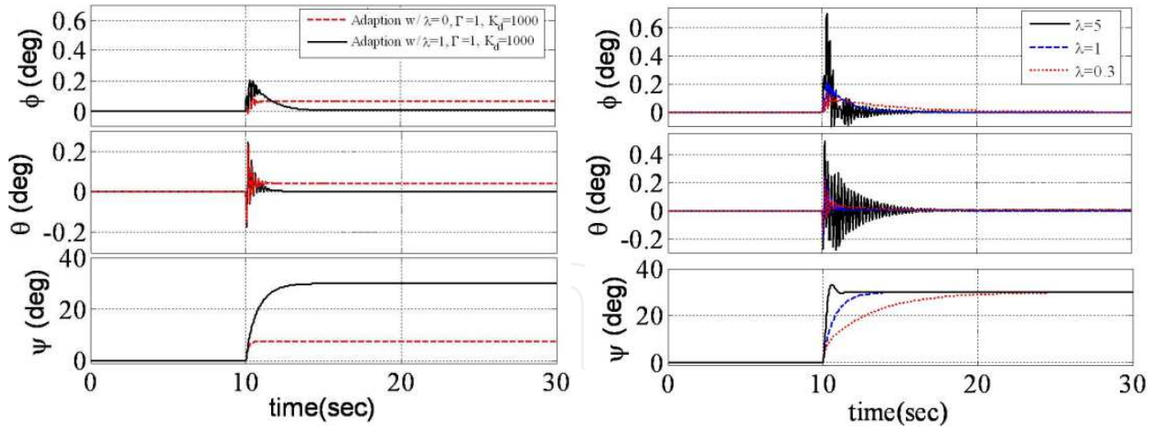

Fig. 20. LEFT: Indirect adaptive control with and without reference trajectory. RIGHT: Effects of scale constant λ on indirect adaptive control with reference trajectory.

9.6 Adaption with reference trajectory

Having established adaptive feedforward control is most effective with a reference trajectory; the following section iterates the design scale constant, λ. As seen in Figure 20, lower values of scale constant, λ result in slower controlled response. As λ is increased, system response is faster, but oscillations are increased. Scale constant value between one and five result in good performance preferring a value closer to one to avoid the oscillatory response.

10. Conclusions

Physics based control is a method that seeks to significantly incorporate the dominant physics of the problem to be controlled into the control design. Some components of the methods include elimination of zero-virtual reference, observers for sensor replacements, manipulated input decoupling, and disturbance-input estimation and decoupling. As pointing requirements have become more stringent to accomplish military missions in space, decoupling dynamic disturbance torques is an attractive solution provided by the physics-based control design methodology. Approaches demonstrated in this paper include elimination of virtual-zero references, manipulated input decoupling, sensor replacement and disturbance input decoupling. This paper compares the performance of the physics-based control to control methods found in the literature typically including cascaded control topology and neglecting factors such as back-emf. Another benefit of using the dynamics derived from the predominant physics of the controlled system lies in that an idealized feedforward results that can easily be augmented with adaptive technique to learn a better command while on-orbit and also assist with system identification. .

11. References

[1] C. J. Kempf and S. Kobayashi, "Disturbance observer and feedforward design of a high-speed direct-drive positioning table", IEEE Trans. On Control Systems Tech., vol. 7, no. 5, Sep., 1999.

[2] Tesfaye, H. S. Lee and M. Tomizuka, "A sensitivity optimization approach to design of a disturbance observer in digital motion control systems", IEEE/ASME Trans. on Mechatronics, vol. 5, no. 1, March, 2000.

[3] K.K. Tan, T. H. Lee, H. F. Dou, S. J. Chin, and Shao Zhao, "Precision motion control with disturbance observer for pulsewidth-modulated-driven permanent-magnet linear motors," IEEE Trans. on Magnetics, vol. 39, no. 3, May, 2003.
[4] C. J. Kempf and S. Kobayashi, "Disturbance observer and feedforward design of a high-speed direct-drive positioning table", *IEEE Trans. on Control Systems Tech.*, vol. 7, no. 5, Sep., 1999.
[5] Tesfaye, H. S. Lee and M. Tomizuka, "A sensitivity optimization approach to design of a disturbance observer in digital motion control systems", *IEEE/ASME Trans. on Mechatronics*, vol. 5, no. 1, March, 2000.
[6] K.K. Tan, T. H. Lee, H. F. Dou, S. J. Chin, and Shao Zhao, "Precision motion control with disturbance observer for pulsewidth-modulated-driven permanent-magnet linear motors," *IEEE Trans. on Magnetics*, vol. 39, no. 3, May, 2003.
[7] S. M. Yang and Y. J. Deng, "Observer-based inertia identification for auto-tuning servo motor-drives", in *Industry Applications Conference*, vol. 2, 2005, pp. 968-972.
[8] M. Z. Liu, T. Tsuji, and T. Hanamato, "Position control of magnetic levitation transfer system by pitch angle," *Journal of Power Electronics*, vol. 6, no. 3, July 2006.
[9] T. Ohmae, T. Matsuda, K. Kaniyama, and M. Tachikawa, "A microprocessor-controlled high-accuracy wide-range speed regulator for motor drives," *IEEE Trans. on Ind. Electron.*, vol. 29, no. 3, August, 1982.
[10] J. K. Kim, J. W. Choi, and S. K. Sul, "High performance position control of linear permanent magnet synchronous motor for surface mount device in placement system," in *Conf. Rec. PCC-Osaka*, vol. 1, 2002, pp. 37-42.
[11] Yoo, Y. D. Yoon, S. K. Sul, M. Hisatune, and S. Morimoto, "Design of a current regulator with extended bandwidth for servo motor drive," in *Conf. Rec. PCC-Nagoya*, 2007.
[12] Y. D. Yoon, E. Jung, A. Yoo, and S. K. Sul, "Dual observers for the disturbance rejection of a motion control system," in *Conf. Rec. 42nd IAS Annual Meeting*, 2007, pp. 256-261.
[13] Topographies taken from ME746 course notes, University of Wisconsin at Madison
[14] S. M. Yang, Y. J. Deng, "Observer-based inertial identification for auto-tuning servo motor drives," in *Industry Application Conference*, vol. 2, 2005, pp. 968-972.
[15] Ahmed, J. "Asymptotic Tracking of Spacecraft Attitude Motion with Inertia Identification", *AIAA Journal of Guidance, Dynamics and Control*, Sep-Oct 1998.
[16] Cristi, R., "Adaptive Quaternion Feedback Regulation for Eigenaxis Rotation", *AIAA Journal of Guidance, Dynamics and Control*, Nov-Dec 1994.
[17] Sanya, A. "Globally Convergent Adaptive Tracking of Spacecraft Angular Velocity with Inertia Identification", *Proceedings of IEEE Conference of Decision and Control*, 2003.
[18] Niemeyer, G. and Slotine, J.J.E, "Performance in adaptive manipulator control", *Proceedings of 27th IEEE Conference on Decision and Control*, Decemebr, 1988.
[19] Slotine, J.J.E. and Benedetto, M.D.Di, "Hamiltonian Adaptive Control of Spacecraft", *IEEE Transactions on Automatic Control*, Vol. 35, pp. 848-852, July 1990.
[20] Fossen, T. "Comments on 'Hamiltonian Adaptive Control of Spacecraft' ", *IEEE Transactions on Automatic Control*, Vol. 38., No. 4, April 1993.

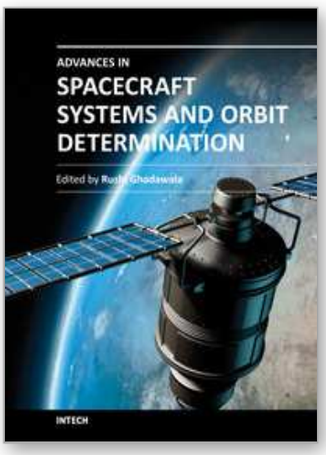

Advances in Spacecraft Systems and Orbit Determination

Edited by Dr. Rushi Ghadawala

ISBN 978-953-51-0380-6
Hard cover, 264 pages
Publisher InTech
Published online 23, March, 2012
Published in print edition March, 2012

"Advances in Spacecraft Systems and Orbit Determinations", discusses the development of new technologies and the limitations of the present technology, used for interplanetary missions. Various experts have contributed to develop the bridge between present limitations and technology growth to overcome the limitations. Key features of this book inform us about the orbit determination techniques based on a smooth research based on astrophysics. The book also provides a detailed overview on Spacecraft Systems including reliability of low-cost AOCS, sliding mode controlling and a new view on attitude controller design based on sliding mode, with thrusters. It also provides a technological roadmap for HVAC optimization. The book also gives an excellent overview of resolving the difficulties for interplanetary missions with the comparison of present technologies and new advancements. Overall, this will be very much interesting book to explore the roadmap of technological growth in spacecraft systems.

INTECH
open science | open minds

InTech Europe
University Campus STeP Ri
Slavka Krautzeka 83/A
51000 Rijeka, Croatia
Phone: +385 (51) 770 447
Fax: +385 (51) 686 166
www.intechopen.com

InTech China
Unit 405, Office Block, Hotel Equatorial Shanghai
No.65, Yan An Road (West), Shanghai, 200040, China
中国上海市延安西路65号上海国际贵都大饭店办公楼405单元
Phone: +86-21-62489820
Fax: +86-21-62489821

IntechOpen